SUPPLEMENTAL INFORMATION

Supplemental Figure S1, associated with Table 1 and Figure 1

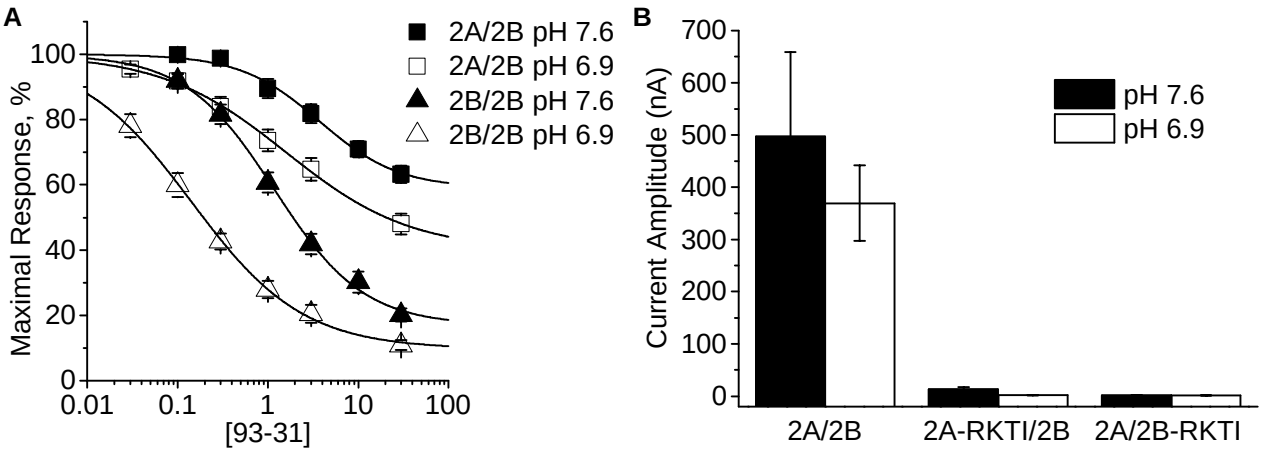

Proton-sensitive inhibition of triheteromeric GluN1/GluN2A/GluN2B NMDA receptors by 93-31. **A**) Concentration-response curves for 93-31 were generated for current responses of GluN1/2A/2B* (2A/2B) and GluN1/2B/2B* (2B/2B) receptors to maximal concentrations of glutamate and glycine at pH 7.6 and pH 6.9 (*n*=7 – 10 oocytes; data represents the mean ± SEM). The 93-31 IC_{50} value at pH 6.9 shifted from 0.14 μM (90% maximal inhibition, n=6) for GluN1/GluN2B/GluN2B* receptors to 1.6 μM (52% maximal inhibition, n=10) for GluN1/GluN2A/GluN2B* receptors. The 93-31 IC_{50} value at pH 7.6 shifted from 1.2 μM (80% maximal inhibition, n=7) for GluN1/GluN2B/GluN2B* receptors to 3.7 μM (37% maximal inhibition, n=10) for GluN1/GluN2A/GluN2B* receptors. **B**) The amplitude of the current contributed by diheteromeric GluN1/2A/2A* and GluN1/2B/2B* receptors that escaped the ER was measured in oocytes expressing GluN1/2A/2B-RKTI* and GluN1/2A-RKTI/2B*, respectively (Hansen et al. 2014). Because the RKTI mutations block glutamate binding, the only active NMDA receptors would contain either two copies of GluN2A* or two copies of GluN2B* receptors that escape ER retention. The amplitude of GluN1/2A/2B-RKTI* (pH 7.6: 1.8 ± 0.5 nA, pH 6.9: 1.4 ± 0.3 nA) and GluN1/2A-RKTI/2B* (pH 7.6: 13 ± 4.5 nA, pH 6.9: 1.6 ± 0.8 nA) current responses were less than 3.5% of GluN1/2A/2B* current responses (pH 7.6: 497 ± 162 nA, pH 6.9: 370 ± 72 nA).

Supplemental Figure S2, associated with Figure 3

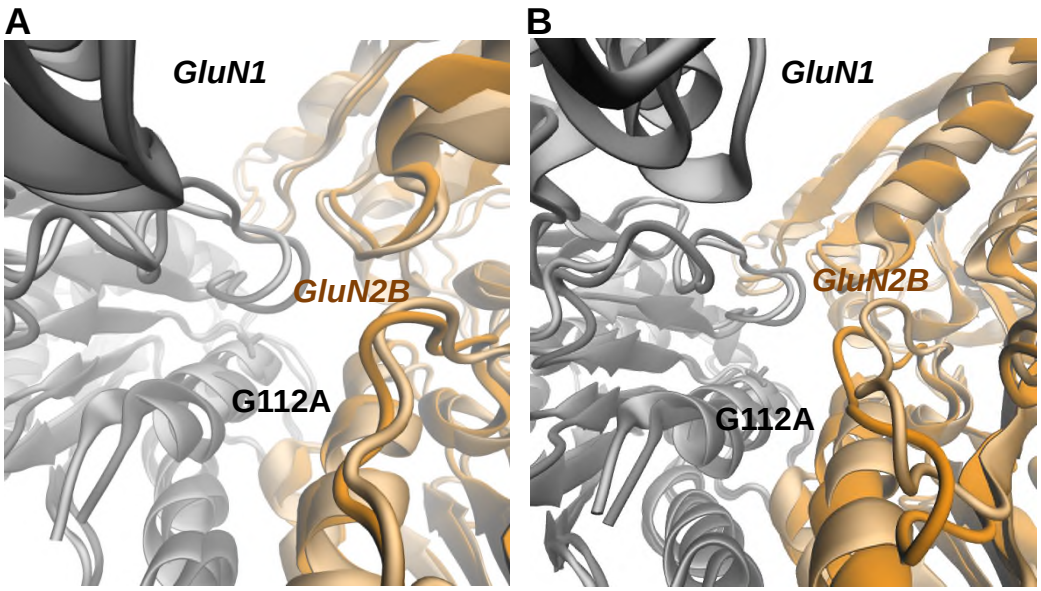

Molecular dynamics simulation of G112A reveals no significant distortions at the GluN1/GluN2B amino terminal domain interface. **A**) The modeled protein structure at 4.8 ns (dark gray/orange) of molecular dynamics simulation for GluN1/GluN2B(G112A) is superimposed on the 0 ns starting position (light gray/orange). **B**) The modeled structure after 4.8 ns (dark gray/orange) of GluN1/GluN2B(G112A) simulation is superimposed on wild-type GluN1/GluN2B. Molecular modeling was performed using Desmond 3.7 from the Schrödinger Software Suite using default parameters.

Supplemental Figure S3, associated with Figure 4

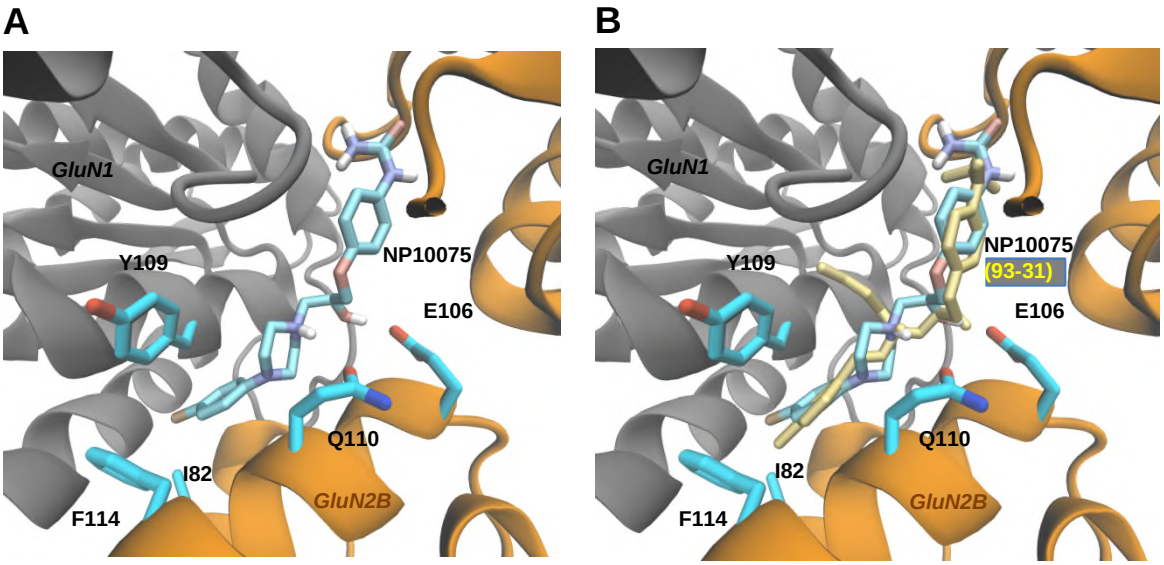

Induced fit docking of NP10075. **A**) The hydroxyl group in NP10075 is predicted to be able to interact with Glu106, similar to 93-3.1. **B**) The same pose for NP10075 depicted in (**A**) overlayed with 93-31 (yellow).

Supplemental Figure S4 , associated with Figure 5

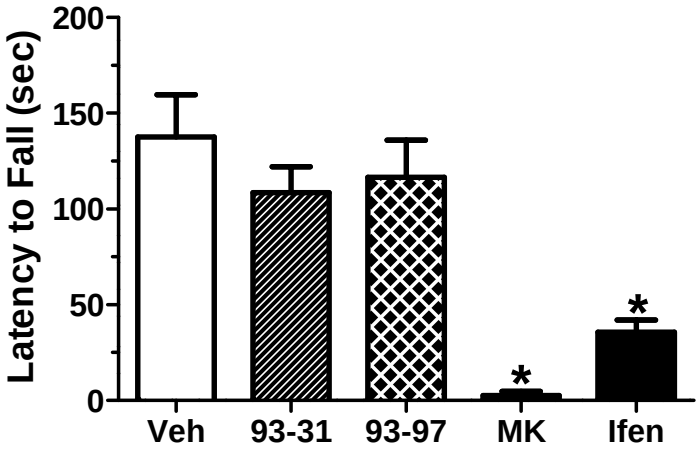

Effect of 93-31 and 93-97 on mouse rotorod performance. Adult male C57BL/6 mice (*Methods*) were trained on the rotorod on consecutive days (4 trials/day, 25 min interval; each day 24 hr interval; 2 days). On day 3 mice were randomly assigned to treatment groups and drugs administered IP in a blinded fashion; vehicle (Veh), 30 mg/kg 93-31, 30 mg/kg 93-97, 30 mg/kg ifenprodil (Ifen), or 0.6 mg/kg (+)MK-801 (MK). The four rotorod trials on day 3 (post drug treatment) were averaged for each mouse. The results shown are the mean $\pm$ SEM per treatment group (n=6 for Veh, 93-31, and 93-97; n=5 for Ifen and MK). One-WAY-ANOVA and Dunnett's test; *$p<0.05$ from vehicle.

Supplemental Table S1, associated with INTRODUCTION: Literature supporting elevation of glutamate in injured tissue in animal models and human patients.

Authors	Journal	Title
Benveniste, H., Drejer, J., Schousboe, A. & Diemer, N. H.	J Neurochem 43, 1369–1374 (1984)	Elevation of the extracellular concentrations of glutamate and aspartate in rat hippocampus during transient cerebral ischemia monitored by intracerebral microdialysis
Baethmann, A. et al.	J. Neurosurg. 70, 578–91 (1989)	Release of glutamate and of free fatty acids in vasogenic brain edema
Choi, D. W. & Rothman, S. M.	Annu. Rev. Neurosci. 13, 171–82 (1990)	The role of glutamate neurotoxicity in hypoxic-ischemic neuronal death.
Nilsson, P., Hillered, L., Ponten, U. & Ungerstedt, U.	J Cereb Blood Flow Metab 10, 631–637 (1990)	Changes in cortical extracellular levels of energy-related metabolites and amino acids following concussive brain injury in rats
Beal, M. F.	FASEB J 6, 3338–3344 (1992)	Mechanisms of excitotoxicity in neurologic diseases
Adachi, H., Fujisawa, H., Maekawa, T., Yamashita, T. & Ito, H.	Int. J. Hyperthermia 11, 587–99 (1995)	Changes in the extracellular glutamate concentrations in the rat cortex following localized by hyperthermia
Rodríguez-Ithurralde, D., Olivera, S., Vincent, O. & Maruri, A.	J Neurol Sci 152 Suppl, S54–S61 (1997)	In vivo and in vitro studies of glycine- and glutamate-evoked acetylcholinesterase release from spinal motor neurones: implications for amyotrophic lateral sclerosis/motor neurone disease pathogenesis
Qureshi, A. I. et al.	Crit Care Med 31, 1482–1489 (2003)	Extracellular glutamate and other amino acids in experimental intracerebral hemorrhage: an in vivo microdialysis study
Kostandy, B. B.	Neurol Sci 33, 223–237 (2012)	The role of glutamate in neuronal ischemic injury: the role of spark in fire
Bondoli, A., Barbi, S., Camaioni, D., Della Morte, F. & Magalini, S. I.	Resuscitation 9, 119–124 (1981)	Plasma and cerebrospinal fluid free amino acid concentration in post-traumatic cerebral oedema in patients with shock
Robertson, C. S. et al.	J Trauma 28, 1523–1532 (1988)	Alterations in cerebral availability of metabolic substrates after severe head injury
Persson, L. & Hillered, L.	J Neurosurg 76, 72–80 (1992)	Chemical monitoring of neurosurgical intensive care patients using intracerebral microdialysis
Baker, A. J., Moulton, R. J., MacMillan, V. H. & Shedden, P. M.	J Neurosurg 79, 369–372 (1993)	Excitatory amino acids in cerebrospinal fluid following traumatic brain injury in humans
Yamamoto, T. et al.	Acta Neurochir Suppl 75, 17–19 (1999)	CSF and ECF glutamate concentrations in head injured patients
Srinivasan, R., Sailasuta, N., Hurd, R., Nelson, S. & Pelletier, D.	Brain 128, 1016–1025 (2005)	Evidence of elevated glutamate in multiple sclerosis using magnetic resonance spectroscopy at 3T
Wagner, A. K. et al.	Crit Care Med 33, 407-413 (2005)	Gender associations with cerebrospinal fluid glutamate and lactate/pyruvate levels after severe traumatic brain injury

Supplemental Table S3, associated with INTRODUCTION: Clinical literature testing glutamate antagonists in cerebral injury.

Authors	Journal	Title
Grotta, J. et al.	Stroke 26, 602–605 (1995)	Safety and tolerability of the glutamate antagonist CGS 19755 (Selfotel) in patients with acute ischemic stroke. Results of a phase IIa randomized trial
Davis, S. M., Albers, G. W., Diener, H. C., Lees, K. R. & Norris, J.	Lancet 349, 32 (1997)	Termination of Acute Stroke Studies Involving Selfotel Treatment. ASSIST Steering Committee
Lees, K. R.	Neurology 49, S66–S69 (1997)	Cerestat and other NMDA antagonists in ischemic stroke
Muir KW.	Curr Opin Pharmacol 6, 53-60 (2006)	Glutamate-based therapeutic approaches: clinical trials with NMDA antagonists
Farin A, Marshall LF.	Acta Neurochir Suppl, 89, 101-107 (2004)	Lessons from epidemiologic studies in clinical trials of traumatic brain injury
Morris, G. F. et al.	J Neurosurg 91, 737–743 (1999)	Failure of the competitive N-methyl-D-aspartate antagonist Selfotel (CGS 19755) in the treatment of severe head injury: results of two phase III clinical trials. The Selfotel Investigators
The North American Glycine Antagonist in Neuroprotection (GAIN) Investigators."	Stroke 31, 358–365 (2000)	Phase II studies of the glycine antagonist GV150526 in acute stroke: the North American experience. The North American Glycine Antagonist in Neuroprotection (GAIN) Investigators
Albers, G. W., Goldstein, L. B., Hall, D. & Lesko, L. M.	JAMA 286, 2673–82 (2001)	Aptiganel hydrochloride in acute ischemic stroke: a randomized controlled trial
Sacco, R. L. et al.	JAMA 285, 1719–1728 (2001)	Glycine antagonist in neuroprotection for patients with acute stroke: GAIN Americas: a randomized controlled trial
Ikonomidou, C. & Turski, L.	Lancet Neurol 1, 383–386 (2002)	Why did NMDA receptor antagonists fail clinical trials for stroke and traumatic brain injury?
Warach, S. et al.	Cerebrovasc Dis 21, 106–111 (2006)	Effect of the Glycine Antagonist Gavestinel on cerebral infarcts in acute stroke patients, a randomized placebo-controlled trial: The GAIN MRI Substudy
Yurkewicz, L., Weaver, J., Bullock, M. R. & Marshall, L. F.	J Neurotrauma 22, 1428–1443 (2005)	The effect of the selective NMDA receptor antagonist traxoprodil in the treatment of traumatic brain injury.
Lees K.R., Dyker A.G., Sharma A., Ford G.A., Ardron M.E., & Grosset D.G.	Stroke 32, 466-472 (2001)	Tolerability of the low-affinity, use-dependent NMDA antagonist AR-R15896AR in stroke patients: a dose-ranging study
Diener H.C., AlKhedr A., Busse O., Hacke W., Zingmark P.H., Jonsson N., & Basun H.	J Neurol 249, 561-568 (2002)	Treatment of acute ischaemic stroke with the low-affinity, use-dependent NMDA antagonist AR-R15896AR. A safety and tolerability study

Supplemental Table S4, associated with Figure 1: pH-dependence of GluN1/GluN2B association rates for 93-31

	pH 6.9	pH 7.6	pH 7.6 / pH 6.9	N [e]
k_{ON}, $M^{-1}s^{-1}$ [a]	0.2141 x 10^6	0.06731 x 10^6	0.31	19,20
k_{OFF}, s^{-1} [b]	0.1084±0.002	0.3514±0.002	3.24	15,9
K_D, nM [c]	506	5220	10.3	--
IC_{50}, nM (HEK cells) [d]	40	360	9.0	4-6

[a] k_{ON} was determined from the slope of the linear regression for the composite plot of 1 / tau_{ONSET} of inhibition against 93-31 concentration (see *Results* and Fig 1d in the main text).

[b] k_{OFF} was determined from the y-intercept of the linear regression for the composite plot of 1 / tau_{ONSET} of inhibition against 93-31 concentration (see *Results* and Fig 1d in the main text).

[c] K_D was calculated from k_{OFF} / k_{ON}.

[d] IC_{50} values in HEK cells were from Figure 1b.

[e] N is the number of independent HEK cells tested (pH 6.9, pH 7.6). All experiments were performed in maximally-effective concentration of glutamate (100 μM) and glycine (30 μM) on rat GluN1/GluN2B receptors.

Supplemental Table S5, associated with Figure 5: Pharmacokinetics of 93-31 in rodents.

Species[a]	Route[b]	Dose (mg/kg)	Cmax [c] (ng/mL)N	Tmax (hr)	AUC_{inf} (hr*ng/mL)	$T_{1/2}$ (hr)	Brain: Plasma Ratio (N)	Study [d]
Mouse	IP	1	165 ± 34 (3)	0.08	203	0.7	-	A
Mouse	IP	3	592 ± 15 (3)	0.08	674	1.0	-	A
Rat	IV	4	590 ± 50 (3)	0.08	514	0.9	1.2 ± 0.2 (9)	B
Rat	IV	10	2577 ± 196 (3)	0.08	2188	1.4	-	C

[a] Mouse strain was C57BL/6. Rat strain was Sprague-Dawley.
[b] Route of drug administration: intraperitoneal, IP; intravenous, IV.
[c] Data shown are from a minimum of n=3 per data point. Mean ± SEM.
[d] Study A formulation was 1:1 DMSO:saline. Study B and C formulation was 2% dimethylacetamide: 98% (2-hydroxypropyl)-β-cyclodextrin (5% in water).

Supplemental Table S6, associated with DISCUSSION and Table 1: pH dependence of known NMDAR antagonists at recombinant GluN1/GluN2B.

Drug	pKa [a]	Fold increase in ionized species [b]	IC_{50} pH 6.9 [c] μM (N)	IC_{50} pH 7.6 [c] μM (N)	IC_{50}(7.6) / IC_{50}(6.9)
Ifenprodil [d]	9.5	1.0	0.075 (39)	0.13 (33)	1.7
Eliprodil [d]	8.4	1.1	0.23 (43)	0.88 (49)	3.8
CP-101,606 [d]	8.8	1.1	0.021 (42)	0.014 (44)	0.7
Radiprodil [d]	9.2	1.0	0.006 (25)	0.011 (42)	1.8
Ro 8-4304 [d]	7.5	1.8	0.58 (20)	1.40 (12)	2.4
Ro 25-6981 [d]	9.4	1.0	0.013 (38)	0.012 (36)	0.9
Ro 63-1908 [d]	8.7	1.1	0.047 (10)	0.21 (9)	4.6
Haloperidol	8.0	1.3	2.7 (32)	9.6 (30)	3.6
Compound 52 [d,e]	8.0	1.3	0.015 (24)	0.065 (26)	4.3
Clobenpropit	7.3, 7.6	1.1	0.55 (8)	0.80 (9)	1.5
Iodophenpropit	7.3, 8.3	1.3	0.33 (10)	1.1 (10)	3.3
NP10075 [d,f]	6.9, 2.8 [g]	3.0	0.045 [f]	0.43 [f]	9.1 [f]

[a] The pKa of the chain nitrogen was calculated using ACD/pKa DB 12.00, www.acdlabs.com.
[b] The fold change in ionized species at pH values 6.9 and 7.6 were calculated as the ratio of the dominant mono-cationic species at the two pH values, as described in Table 1.
[c] IC_{50} values for inhibition of GluN1/GluN2B expressed in *Xenopus* oocytes were determined as described in the *Methods* from composite inhibition curves at different pH values. pH has minimal effects on EC_{50} values for either glutamate or glycine (Traynelis et al 1995). The number of oocytes (N) recorded is shown in parentheses.
[d] Data from human GluN1 and human GluN2B.
[e] Compound 52 is from Mosley et al. 2009.
[f] Data reported by Wang et al. 2014 are included for comparison.
[g] Predicted pKa values for piperazine nitrogens distal and proximal to the adjacent phenyl ring; predicted pKa values for the urea nitrogens were above 11 and are not given. Ionization was calculated for distal nitrogen.

SUPPLEMENTAL EXPERIMENTAL PROCEDURES

HEK cell preparation and transfection

HEK 293 cells (CRL 1573; ATCC, Rockville, MD; hereafter HEK cells) were plated onto glass coverslips (5 mm diameter, Warner Instruments, Hamden, CT) coated with 0.1 mg/ml poly-D-lysine. HEK cells were maintained in 5% humidified CO_2 at 37ºC in DMEM (Dulbecco's Modified Eagle Medium, Cat. No. 11960; Invitrogen) supplemented with 10% fetal bovine serum, 10 units/ml penicillin, and 10 μg/ml streptomycin. HEK cells were transiently transfected using the Fugene 6 transfection reagent (Roche Diagnostics, Indianapolis, IN) with cDNAs encoding green fluorescent protein (GFP), GluN1-1a, and GluN2B at a ratio of 1:1:1 and 0.5 μg/well total cDNA for 16-24 hours before whole cell voltage-clamp recordings. Following transfection, cells were incubated in media supplemented with NMDAR antagonists D,L-2-amino-5-phosphonovalerate (D,L-APV, 200 μM) and 7-chlorokynurenic acid (7-CKA, 200 μM).

Triheteromeric GluN1/GluN2A/GluN2B receptors

The GluN2A and GluN2B subunits were fused to C-terminal peptides (C1 or C2) containing the $GABA_{B1}$ (C1) or $GABA_{B2}$ (C2) coiled-coil domains and a dilysine ER retention sequence. The C1 and C2 tags form a coiled-coil structure that masks the ER retention signal, thus allowing selective surface expression of tetramers containing one C1-tagged subunit and one C2-tagged subunit. Oocytes were injected with cRNA encoding GluN1-1a, $GluN2A_{C2}$ and $GluN2B_{C1}$, or GluN1, $GluN2B_{C1}$ and $GluN2B_{C2}$ (referred to as GluN1/2A/2B* and GluN1/2B/2B* in Figure S1). The mutated subunits used in Figure S1B were GluN2A-R518K + $T690I_{C2}$ and GluN2B-R519K + $T691I_{C1}$ (referred to as GluN2A-RKTI* and GluN2B-RKTI*).

Pharmacokinetics in rodents

Sprague-Dawley rats were dosed with either 4 or 10 mg/kg IV for plasma pharmacokinetics, formulated in 2% dimethylacetamide: 98% (2-hydroxypropyl)-β-cyclodextrin (5% in water). Animals were fasted overnight prior to dosing, and food returned to the animals two hours after dosing. Blood and brain tissue samples were collected at regular time intervals (n=3 at each time). Plasma samples were prepared immediately after collection by centrifugation for ten minutes, and the supernatant stored below -20°C. Brain tissue was weighed, homogenized on ice in 50 mM K-phosphate buffer and the homogenate was stored below -20°C until analysis. Plasma and brain homogenate samples were extracted by the addition of 5 volumes of cold acetonitrile, mixed well by vortexing and centrifuged at 4000 rpm for 15 minutes. The supernatant fractions were analyzed by LC-MS/MS operating in multiple reaction monitor mode (MRM). The amount of parent compound in each sample was calculated by comparing the response of the analyte in the sample to that of a standard curve (Ricerca, OH). C57BL/6 mice were dosed at 1 and 3 mg/kg (50% DMSO: 50% saline) by IP and plasma samples collected over a 24 hr period and prepared similar as above (Davos, NJ) to determine plasma pharmacokinetic endpoints.